THE JOURNAL OF PHYSICAL CHEMISTRY C

Article

pubs.acs.org/JPCC

Computational Design of New Magnesium Electrolytes with Improved Properties

Xiaohui Qu,[†,#] Yong Zhang,[‡,#] Nav Nidhi Rajput,[†] Anubhav Jain,[†] Edward Maginn,[‡] and Kristin A. Persson[*,†,§]

[†]Energy Technologies Area, Lawrence Berkeley National Laboratory, Berkeley, California 94720, United States

[‡]Department of Chemical and Biomolecular Engineering, University of Notre Dame, Notre Dame, Indiana 46556, United States

[§]Department of Materials Science and Engineering, University of California Berkeley, Berkeley, California 94704, United States

Supporting Information

ABSTRACT: In this work, we use computational design to examine 15 new electrolyte salt anions by performing chemical variations and mutations on the bis(trifluoromethane)sulfonamide (TFSI) anion. On the basis of our calculations, we propose two new anions as potential candidates for magnesium energy-storage systems, which are evolved from TFSI with the substitution of sulfur atoms in TFSI and the modification of functional groups. The applicability of these new anion salts is examined through comprehensive calculations using both first-principles as well as benchmarked classical molecular dynamics. We elucidate the important properties of these anions, including the electrochemical stability window, chemical decomposition, preferred solvation structure, diffusion coefficient, and other dynamical properties for 15 rationally designed molecules. Two of the designed anions are found to successfully avoid the vulnerability of TFSI during ion-pair charge-transfer reactions while retaining comparable or better performance of other properties. As such, our work provides, to our knowledge, the first theoretically designed electrolyte salt for contemporary multivalent batteries and provides guidance for the synthesis and testing of novel liquid electrochemical systems.

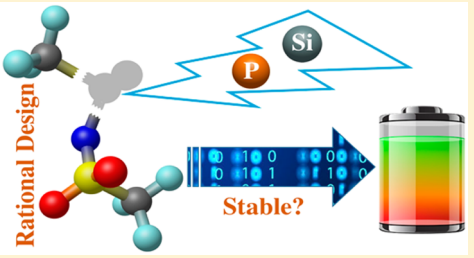

1. INTRODUCTION

A wide variety of important technologies rest on improved understanding and advancement of new electrolytes with optimized properties. Current, as well as future, energy-storage solutions critically depend on the stability of the electrolyte, which governs the electrochemical window of viable electrode-pairs. For example, Li-ion intercalation cathodes are limited by the anodic stability of current salts/solvents, and the negative electrode usually forms a functional passivation layer, with selective ion transport, which allows the electrolyte to operate outside of its thermodynamic stability. Today, no organic solvent is known that remains stable under Li-oxygen electrochemical operations.[1−3] Furthermore, efficient multivalent-metal anode plating and stripping is generally restricted to corrosive halide-containing electrolytes.[4−7] The lack of fundamental understanding of the correlations between properties and the underlying atomistic interactions—both in the bulk electrolyte as well as at the electrode interface—is inhibiting a rational design of novel electrolytes. In this work, we demonstrate, for the first time, a computational framework to design novel electrolyte salts, specifically targeting increased cathodic stability in a multivalent energy-storage system. Multivalent energy storage, based on divalent ions such as Mg^{2+} and Ca^{2+}, provides an interesting approach to achieve higher energy density than existing Li-ion solutions. In particular, magnesium metal has attracted attention[8−13] due to its volumetric capacity, which is greater than a lithium graphite anode (3833 mA h cm^{-3} vs 2046 mA h cm^{-3}),[14] and the seminal proof of concept work by the Aurbach group.[8,15−19]

Most conventional salts used in Li-ion systems, e.g., PF_6^-, ClO_4^-, AsF_6^-, exhibit high anodic stability,[8,20] but are unstable against Mg metal, such that a passivating ion-blocking layer, incompatible with reversible electrochemical operations, is formed from the decomposition of the electrolyte at the anode surface.[8,15,16,18,21,22] Recently, encouraging results have been reported on carborane salts as well as $Mg(TFSI)_2$.[11,23] However, in the case of $Mg(TFSI)_2$, experimental studies present conflicting evidence on its cathodic stability and compatibility with the Mg metal. For example, it is observed that the electrochemical reversibility of $Mg(TFSI)_2$ in diglyme is highly concentration dependent.[11] Previous work by the present authors has elucidated that the strong ion pairing in Mg electrolytes coupled with the multiple-electron charge transfer reaction at the negative electrode provides one possible reason for a concentration-dependent interfacial decomposition reaction in $Mg(TFSI)_2$ systems.[24]

It is worth noting that the same study found the BH_4^- anion to be tolerant to close exposure to transient reduced Mg

Received: May 10, 2017
Revised: June 14, 2017
Published: July 12, 2017

DOI: 10.1021/acs.jpcc.7b04516
J. Phys. Chem. C 2017, 121, 16126−16136

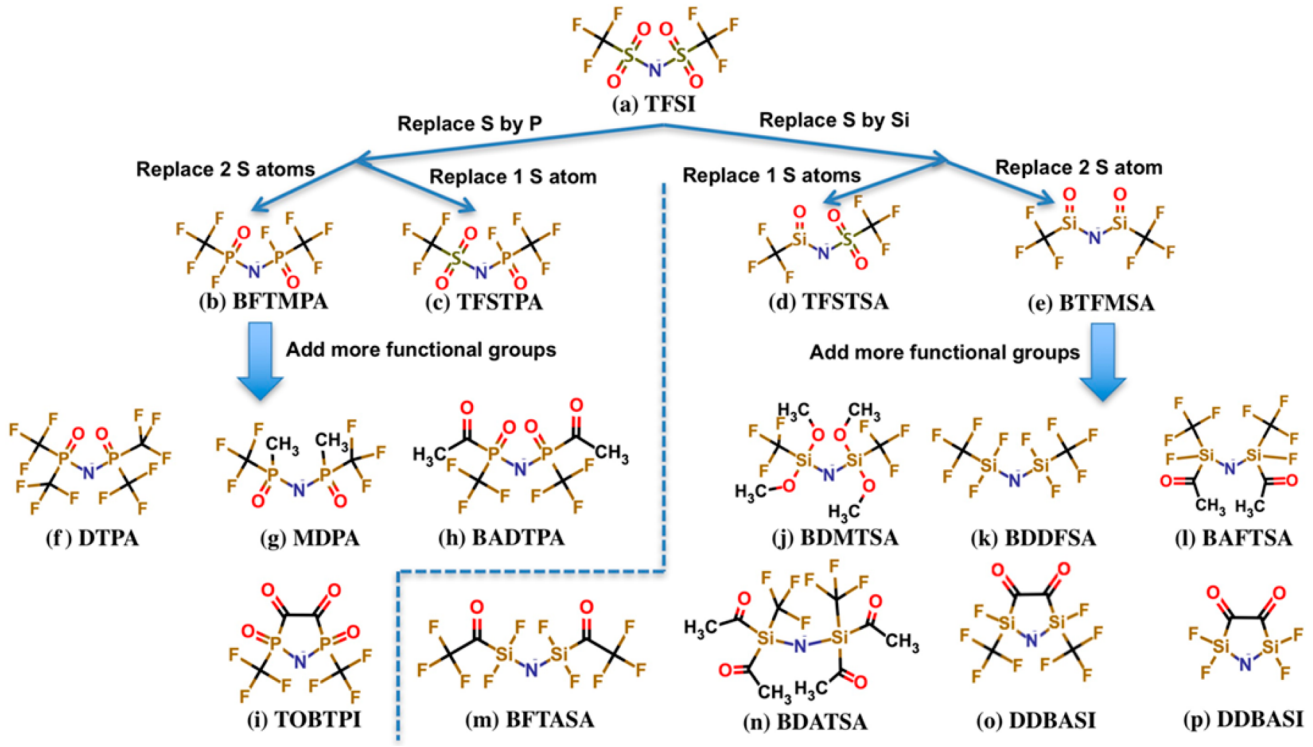

Figure 1. Original "host" TFSI anion and the new anions proposed in this paper. Abbreviations: (a) TFSI: bis(trifluoromethane)sulfonamide; (b) BFTMPA: bis[fluoro(trifluoromethyl)phosphoryl]azanide; (c) TFSTPA: [(trifluoromethane)sulfonyl][fluoro(trifluoromethyl)-phosphoryl]azanide; (d) TFSTSA: [(trifluoromethane)sulfonyl)][(trifluoromethyl)-silyl]azanide; (e) BTFMSA: bis[(trifluoromethyl)silyl]azanide; (f) DTPA: bis-[(ditrifluoromethyl)phosphoryl]azanide; (g) MDPA: bis[methyl(ditrifluoromethyl)phosphoryl]azanide; (h) BADTPA: bis[acetyl-(ditrifluoromethyl)phosphoryl]azanide; (i) TOBTPI: 2,3,4,5-tetraoxo-2,5-bis(trifluoromethyl)-1,2λ^5,5λ^5-azadiphospholidin-1-ide; (j) BDMTSA: bis[dimethoxy(trifluoromethyl)silyl]azanide; (k) BDDFSA: bis[difluoro(trifluoromethyl)silyl]azanide; (l) BAFTSA: bis[acetyl(fluoro)-(trifluoromethyl)silyl]azanide; (m) BFTASA: bis[difluoro(trifluoroacetyl)silyl]azanide; (n) BDATSA: bis[diacetyl(trifluoromethyl)silyl]azanide; (o) DDBASI: 2,5-difluoro-3,4-dioxo-2,5-bis(trifluoromethyl)-1,2,5-azadisilolidin-1-ide; (p) TFDASI: 2,2,5,5-tetrafluoro-3,4-dioxo-1,2,5-azadisilolidin-1-ide.

species. Hence it is expected that the BH_4^--supported electrolytes remain stable under the same conditions, which is indeed confirmed by their performance in Mg metal electrochemistry.[25] Thus, the identification of the specific mechanism and bond-weakening that governs the ability of an electrolyte salt to enable Mg metal plating provides us not only with a plausible explanation for the existing salt performance but also with a unique opportunity to explore and virtually "screen" new anions for a more stable configuration. In this paper, we use our previous insights to design new Mg-electrolyte salts by performing chemical variations and mutations on the TFSI anion to increase its stability for Mg metal-plating operations. All destructive reactions are carefully examined through computational methods with the aim to screen for the best electrolyte anion candidate. Furthermore, we consider not only the electrochemical stability window (ESW) of the resulting salts, but also stability against hydrolysis and bulk electrolyte conductivity as screening metrics for our candidate salts. We note that the current work covers not only the bulk properties, e.g., ESW, hydrolysis and conductivity, but also bonding breaking, which is responsible for the interfacial film formation. However, we also note that some other important properties, such as compatibility with the commonly used steel and Al current collectors,[15,20] are not covered by the current work.

2. PROPOSED ANION CANDIDATES

To explore potentially more-stable chemical varieties of the TFSI anion, we preferentially substitute on the bond that has been known to be weakened, namely, the C−S bond. The proposed 15 new Mg-electrolyte anion structures and corresponding abbreviations are shown in Figure 1. Compounds *b*−*e* (BFTMPA, TFSTPA, TFSTSA, BTFMSA) are first-generation derivatives from TFSI. These are generated by substitution of one or both of the sulfur atoms in TFSI with phosphorus or silicon. To increase the diversity and potentially improve the performance of the candidate pool, second-generation derivatives are generated by adding more functional groups to BFTMPA and TFSTSA, which result in compounds *f*−*p* in Figure 1. In general, we minimize the changes to the molecular size and surface atoms, in order to retain the desirable properties of TFSI, such as its weakly coordinating nature and diffusivity, while improving its stability for Mg plating. The lowest energy conformation is generated using ChemAxon MarvinSketch for all of the proposed 15 new anions.[26]

3. METHODOLOGY

The proposed anions are virtually tested by calculating a range of properties that are critical for battery electrolyte applications, including the electrochemical stability window, chemical stability, hydrolyzing sensitivity, and transport properties. The original anion TFSI features several promising properties, such

DOI: 10.1021/acs.jpcc.7b04516
J. Phys. Chem. C 2017, 121, 16126−16136

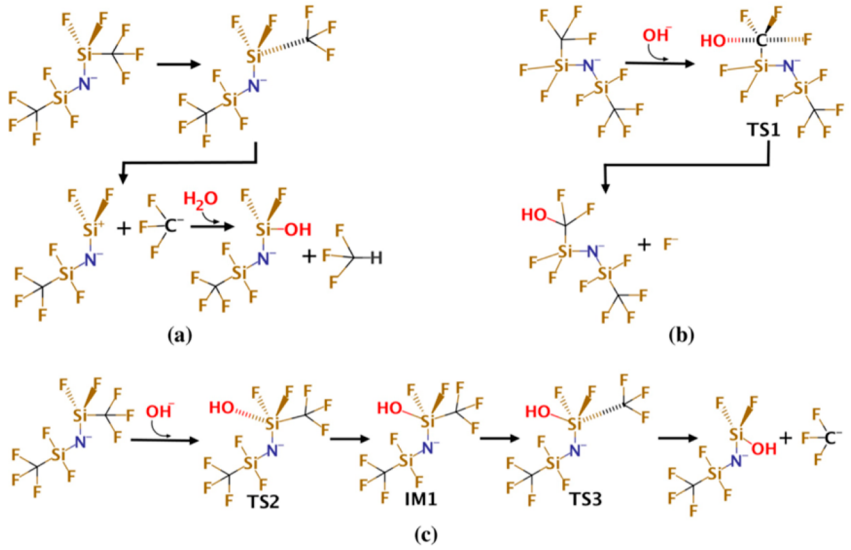

Figure 2. Example hydrolysis mechanisms of BDDFSA. (a) S_N1 mechanism; (b) synchronous S_N2 mechanism; (c) asynchronous S_N2 mechanism. TS1, TS2, and TS3 are transition states, while IM1 is a metastable immediate.

as ESW and diffusivity, which are promising for Mg-electrolyte applications. The target of this work is not to improve these properties but to design new anions that retain the good aspects of TFSI (on ESW, diffusivity, and so on) while being resistant to C−S bond breaking during Mg deposition. The main focus is to identify novel mutations of TFSI with increased stability against association with Mg^{1+}, hence, all noncyclic bonds (such as P−C, C−Si, C−F, etc.) are examined in order to safeguard against possible decomposition modes of the new, rationally designed anions.

The QM simulations are initialized from a Mg-TFSI bidentate structure, in which the Mg^{2+} cation is coordinated by two oxygen atoms from two different sulfur atoms, as confirmed by recent experimental and computational studies.[27,28] Reaction enthalpy and/or barrier heights are calculated to assess the chemical stability and hydrolysis sensitivity. Because there is no unambiguous way to determine the screening criteria of the reaction enthalpy and the barrier height, two reasonably large numbers, 10 kcal/mol (0.43 eV) and 20 kcal/mol (0.87 eV, corresponding to a temperature of 10 065.4 K), are chosen empirically as very high thresholds (34 times k_BT at room temperature) for the reaction enthalpy and the barrier height, respectively, to define strong endothermic and kinetically infeasible reactions.

3.1. Electrochemical Stability Window (ESW). The electrochemical stability window (ESW) is one of the key determinates of an electrolyte and can be related to the ionization potential (IP) and electron affinity (EA), which are correlated to the anodic and cathodic limit, respectively. IP is calculated by the energy gap between the relaxed cation and neutral states, whereas EA is calculated by the energy gap between the relaxed neutral and anion states. We emphasize that this methodology is more stringent than the often-applied one based on the HOMO and LUMO, which represent the energy differences between the rigid molecular orbitals. All stationary points are confirmed as real minima by the exclusion of any imaginary frequencies. All quantum mechanical calculations are performed at the B3LYP/6-31+G* level. The solvent effect is taken into account by the dielectric continuum IEF-PCM model.[29] Benchmark calculations with an explicit solvent model show that the mean absolute error (MAE) of the IEF-PCM approach is less than 0.34 eV for the ESW prediction (see Table S1). We note that the zero-point energy (ZPE) and counterpoise correction is not included. All of the IP/EA calculations were carried out by the Electrolyte Genome high-throughput infrastructure, to which we refer for computational details of the ESW calculation.[24,30,31]

3.2. Chemical Stability. Candidate Mg-electrolyte anions should also be resistant to chemical decomposition in the solutions. Hence, we explored the tendency of direct chemical decomposition by systematically breaking all of the bonds of the anion (one at a time) and calculating the bond dissociation energies (BDEs). The lowest bond dissociation energy is defined as the chemical stability index, with the assumption that the weakest bond determines the chemical stability of the whole molecule. The BDE of bond A−B in a molecule is calculated by BDE = $E_B + E_A - E_{AB}$ where A and B are the fragments separated by the bond A−B and E_A, E_B, and E_{AB} represent the energies of fragment A, fragment B, and the molecule, respectively, before bond breaking. Both geometry optimization and vibrational frequency analysis are carried out at the B3LYP/6-31+G* level, while the same functional is used to evaluate the single-point energy with a slightly larger basis set 6-31++G**. The solvent effect is taken into account by the dielectric continuum IEF-PCM model for single-point energy evaluation. Zero-point energy (ZPE) and counterpoise corrections are not included. It can be seen from Table S1 that the MAE of the IEF-PCM approach is less than 0.04 eV compared to that of the explicit solvent model.

3.3. Hydrolysis. Hydrolysis is the reaction between a molecule and water, in which water breaks one of the molecule's bonds and splits the molecule. Even very dry electrolytes contain trace amounts of water, which can render the salt components (anion or cation) unstable. The hydrolyzing reaction can be blocked by either a high reaction enthalpy or barrier height. As hydrolysis can occur through multiple pathways and multiple steps, a combination index consisting of the reaction enthalpy and barrier height of multiple pathways is used to capture the molecule's sensitivity to hydrolysis. Geometry optimization is carried out at the B3LYP/6-31+G* level, while the same functional is used to evaluate single-point energy with a slightly larger basis set 6-

DOI: 10.1021/acs.jpcc.7b04516
J. Phys. Chem. C 2017, 121, 16126−16136

31++G**. Entropy corrections are obtained from the vibrational frequency analysis at the B3LYP/6-31+G* level to deduce the Gibbs free energy at 298.15 K. We emphasize that all of the hydrolysis reaction energies and barrier heights are calculated using Gibbs free energies. The solvent effect is taken into account by the dielectric continuum IEF-PCM model for the single-point energy evaluation. Table S1 shows that IEF-PCM tends to underestimate the barrier height with MAE of 0.16 eV. Counterpoise correction is not included.

The hydrolytic enthalpy for bond A−B in molecule AB is calculated by

$$\Delta H = \min\left(E_{A-OH} + E_{B-H}, E_{A-H} + E_{B-OH}\right) - \left(E_{A-B} + E_{H_2O}\right)$$

in which (A−OH, B−H) and (A−H, B−OH) are two possible hydrolysis product sets, determined by the two options to attach OH and H to hydrolyze the bond. Both directions are considered in the current work. As long as the hydrolytic enthalpy is sufficiently high (≥10 kcal/mol), we consider the A−B bond thermodynamically stable against hydrolysis.

In the case of a exothermic reaction, further analysis is required. Even if a hydrolytic reaction is exothermic, i.e., thermodynamically feasible, it can be kinetically blocked by a high reaction barrier. Therefore, we explore detailed hydrolytic pathways to calculate the barrier height. Figure 2 exemplifies the pathways we have explored using BDDFSA as an example.

The two most common hydrolytic mechanisms are nucleophilic substitution S_N1 and S_N2.

In the S_N1 mechanism, as shown in Figure 2a, the anion first decomposes to a carbonation intermediate by the elimination of the $-CF_3$ group. In the second step, the carbonation intermediate reacts with a neutral water molecule, after which the final hydrolytic product is formed. The first step is slow and, hence, rate determining. As a unimolecular heterolytic decomposition process, it is expected to be barrierless and endothermic. Hence, the formation enthalpy of the carbonation intermediate is used as the barrier height for the S_N1 mechanism.

In the S_N2 mechanism, the hydrolysis is initiated by the nucleophilic attack of the OH^- anion. In this mechanism, bond formation and breaking can take place either synchronously or asynchronously depending on the bond types. The C−F bond hydrolysis in BDDFSA is a good example of a synchronous S_N2 mechanism. Its reactant, transition state (TS1), and products are illustrated in Figure 2b.

The asynchronous S_N2 mechanism is more complicated, in which two transition states are involved. For the hydrolysis reactions studied in this work, it is very common if the nucleophilic attacking site is P or Si. In this scenario, the hydrolytic reaction is initiated by a bond-formation transition state (Figure 2c, TS2) and forms a metastable complex (Figure 2c, IM1), which proceeds to bond breaking (Figure 2c, TS3) and results in the detachment of the $-CF_3$ functional group. As shown later, both TS2 and TS3 steps can present kinetic bottlenecks for the asynchronous S_N2 mechanism.

To reduce the computational cost, the hydrolysis screening is performed using the following strategy: (1) the reaction enthalpy is calculated for all of the bonds, where strongly endothermic bonds (BDE ≥ 10 kcal/mol) pass the hydrolysis sensitivity screen; (2) a detailed hydrolytic pathway including transition states is obtained for the rest of the bonds. The highest barrier is used for a sequential multiple step pathway, whereas the smallest barrier is used for parallel mechanisms (e.g., S_N1 vs S_N2). Finally, the smallest barrier of all of the bonds is retained as the hydrolysis index for the anion, with the assumption that the minimum barrier pathway provides the most likely mechanism for hydrolysis.

3.4. Liquid Structure and Transport Properties. Finally, transport properties and solvation structures are obtained using classical molecular dynamics (MD) simulations using the LAMMPS package.[32] Simulation details closely follow those described in our previous publications.[33,34] All of the electrolyte solutions are simulated at 0.4 M, and the system sizes used in this work are summarized in Table 1. Six solvents are included:

Table 1. System Sizes Used in the Current Work

solvent	# of cation	# of anion	# of solvent
AN	32	64	1536
THF	25	50	768
DMSO	25	50	902
G1	25	50	604
G2	25	50	437
G4	25	50	277

acetonitrile (AN), tetrahydrofuran (THF), dimethyl sulfoxide (DMSO), dimethoxyethane (G1), diglyme (G2), and tetraglyme (G4). The simulation boxes are equilibrated for 2 ns in the isothermal−isobaric (NPT) ensemble followed by 20 ns production runs in the canonical (NVT) ensemble.

The inter- and intramolecular interactions in the system are described using the general Amber force field (GAFF)[35] unless otherwise specified (see below). Each isolated ion or solvent molecule is optimized at the B3LYP/6-311++G(d,p) level using the Gaussian09 package.[36] The atomic charges are then derived by fitting the electrostatic potential surface using the RESP method.[37] The long-range electrostatic interactions are calculated using the particle-particle particle-mesh (PPPM) method.[38]

For the three glymes, the GAFF force field is found to overestimate the liquid density at 298 K by 4.3−7.4%. Therefore, the force field developed recently by Tsuzuki and co-workers[39] is used for these solvents instead of GAFF. We note that this force field was originally based on the OPLS force field.[40] To be consistent with the GAFF force fields used in the current work, the 1−4 Coulombic interactions are scaled by 5/6 instead of the 1/2 scaling usually used for OPLS force fields. In addition, the Lorentz−Berthelot combination rule is applied instead of the geometric rule used in the OPLS force field. It is found that these changes only marginally affect the simulation results (results not shown). Due to the lack of a reliable force field, the solvent dimethylamine (DMA) is only studied using ab initio calculations and is not studied using the classical MD simulation. For the anion BDMTSA, parameters related to Si are absent in GAFF. The van der Waals parameters for Si are taken from the literature[41] and the partial charges are obtained using the RESP method as described above. The dihedral angle parameters are fitted to ab initio calculations. (The dihedral angle parameters in other anions are also refined following the same procedure). These are the most important parameters to capture the liquid phase structure and dynamics such as self-diffusivity and conductivity. Other parameters (representing bond and angle flexibility) are consistent with the GAFF parameters for phosphorus, which have similar weight and

DOI: 10.1021/acs.jpcc.7b04516
J. Phys. Chem. C 2017, 121, 16126−16136

bond lengths in the optimized structure. The parameters for BDMTSA are provided in the Supporting Information (SI).

4. RESULTS AND DISCUSSION

4.1. Electrochemical Stability Window (ESW). The proposed anions exhibit diverse electrochemical stability behavior. The ESW of the solvent-separated anions is shown in Figure 3 as light green bars. For some species, either the

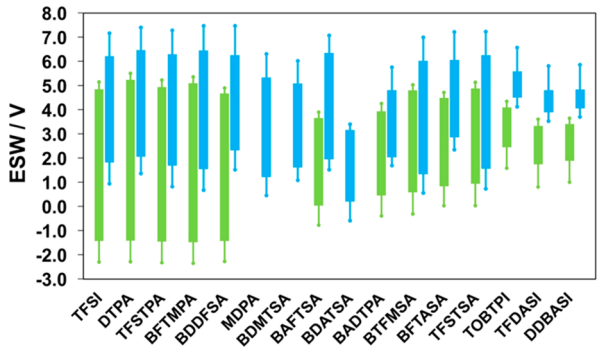

Figure 3. Calculated electrochemical stability windows (ESW) of the "original" TFSI and the proposed derivative anions in different solvents in different chemical environments. All values are reported versus Mg^{2+}/Mg, and the solvent effect is taken into account by the IEF-PCM model.[29] The thick bar represents the range that an anion is stable in all solvents, while the thin "error" bar represents the fluctuations of stability region as a result of the solvent environment. The following solvents are considered: acetonitrile, diglyme, dimethoxyethane, dimethylamine, dimyethyl sulfoxide, tetraglyme, and tetrahydrofuran. Colors represent different first-shell solvation structures. Light green: the well-solvated anion. Light blue: the solvated $[Mg\text{-}Anion]^+$ ion pairs. Missing values are due to irrecoverable failures during calculations.

anodic or cathodic limit fails due to convergence issues, while the other one is successful predicted. While such data are used in the following discussion, it is not shown in Figure 3. The first class of anions, namely, DTPA, TFSTPA, BFTMPA, BDDFSA, MDPA, and BDMTSA, contain only saturated functional groups such as F, CF_3, and OCH_3 and exhibit ESWs similar or better than that of TFSI. They are not only stable at the Mg^{2+}/Mg potential but also associate with a good anodic limit (>4.0 V vs Mg^{2+}/Mg). Another class of anions, including BAFTSA, BDATSA, BADTPA, BTFMSA, and BFTASA, are characterized by ketone or silanone functional groups. Their ESW is marginally stable at the Mg^{2+}/Mg potential. The third class of anions, TOBTPI, TFDASI, and DDBASI, are composed of cyclic structures and exhibit inferior ESW. Therefore, as a general trend for anions proposed in this paper, substitution by F, CF_3, and OCH_3 functional groups is found to be a fruitful strategy to generate candidates with good ESW. In summary, DTPA, TFSTPA, BFTMPA, BDDFSA, MDPA, and BDMTSA show an a priori promising electrochemical stability window for Mg-ion batteries. As a result, only these six anions were studied in the following chemical decomposition and hydrolysis test.

In order to compare to our earlier studies for TFSI,[24] the ESW of ion-paired anions was also calculated and the results are shown in Figure 3 as light blue bars. Similar to our previous study, the $[Mg\text{-}Anion]^+$ ion pair shows a higher reduction potential than the well-solvated anions, and hence, the ion pair will be readily reduced before the well-solvated anion. The Mg^{2+} cation is identified as the reduction center for all ion pairs (e.g., the electron localizes on the cation in the ion pair), and a complexed Mg^+ cation is hypothesized, which is consistent with our previous study.[24] During its lifetime, this transient Mg^+ species can activate the proposed anions to render them susceptible to decomposition, similar to TFSI.[24] Watkins et al.[27] observed that decreasing the tendency of $[Mg\text{-}TFSI]^+$ to form ion pairs by adding 1:1 G4 to $Mg(TFSI)_2$/G2 can improve the electrochemical stability, in which, all of the G4 is expected to coordinate with Mg^{2+}, and no TFSI coordinates with Mg^{2+}. However, adding more G4 was found to jeopardize the oxidative stability. The new anions proposed in the current work aim to provide an alternative solution to improving the anodic stability of the electrolyte while retaining the cathodic stability.

4.2. Chemical Stability. As reported in our earlier study, the $[Mg^+TFSI^-]$ ion pair, followed by formation of Mg^+ cation, is subject to potential decomposition through S−C bond breaking. The six electrochemically stable anions are further screened by calculating the lowest bond dissociation energies (BDE). The results are shown in Figure 4. It is worth noting

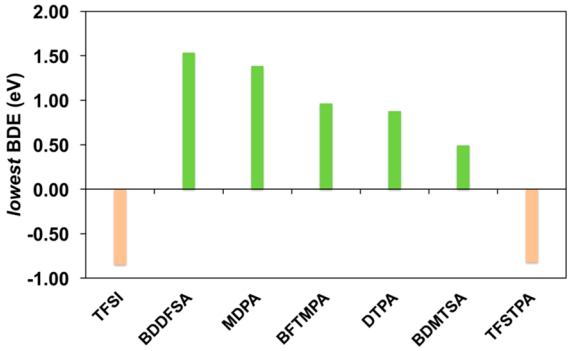

Figure 4. Lowest bond dissociation energy (LBDE) of the "original" TFSI and derived novel anions, considering different first-shell solvation structures including (i) their well-solvated form, (ii) ion paired with Mg^{2+}, and (iii) ion paired with Mg^+. The solvent effect of diglyme is taken into account by the PCM model.

that while S−C is the weakest bond in TFSI, it is not always true for the other anions. Hence, we calculate BDEs for all of the bonds and subsequently identify the weakest bond for each anion.

The proposed anions demonstrate distinctly different chemical stabilities as compared to the original TFSI anion, which is very encouraging. The first class of anions is extremely stable. BDDFSA is representative of this class. The most vulnerable bond for BDDFSA is identified as Si−C in association (e.g., ion-paired) with Mg^+. However, this bond still exhibits a binding energy (BDE) of 1.54 eV which can be considered quite stable. Without the association of the reactive Mg^+, the BDE of BDDFSA is as high as 3.87 eV for the well-solvated anion and as high as 3.44 eV when ion-paired with Mg^{2+}. Therefore, while Mg^+ slightly destabilizes BDDFSA in a way similar to TFSI, the consequence is far from catastrophic. The BDEs for all other bonds in BDDFSA are presented in Supporting Information (Figure S1). The other anions in this class, including MDPA, BFTMPA, and DTPA are associated with a BDE close to 1.0 eV, which is lower but still endothermic. BDMTSA requires a mild energy of 0.49 eV to break its weakest C−O bond. While not as stable as some of the other anions, BDMTSA is still expected to be stable at

DOI: 10.1021/acs.jpcc.7b04516
J. Phys. Chem. C 2017, 121, 16126−16136

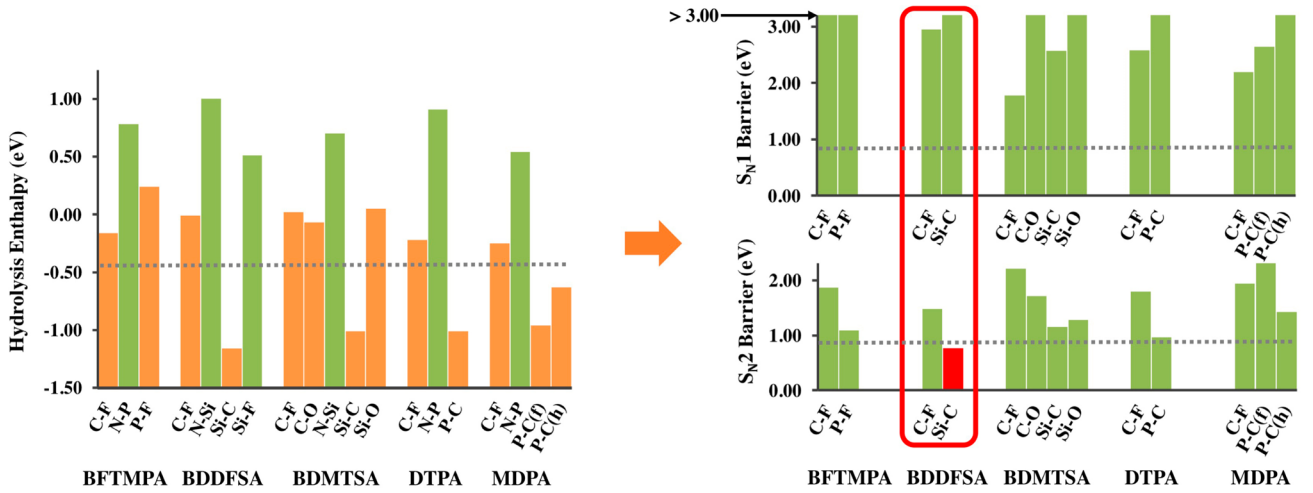

Figure 5. Hydrolytic reaction enthalpy/barrier height. A green color represents a stable bond by enthalpy/barrier height. An orange color represents a marginally stable bond, in which the barrier height is calculated. A red color represents an unstable bond as identified through the minimum barrier height of either the S_N1 or S_N2 mechanism.

room temperatures. While most proposed anions show improved chemical stability, TFSTPA exhibits an exothermic S−C bond when ion paired with the radical Mg^+ cation, similar to the case of the original TFSI.[24] In summary, the decomposition of BDDFSA, MDPA, BFTMPA, DTPA, and BDMTSA are significantly endothermic even in the worst-case scenarios and are considered to be chemically stable under our screening criteria. Hence, these five anions provide potentially interesting candidates for improved chemical stability and comparable electrochemical stability as compared to TFSI by eliminating/substituting the S−C bond.

4.3. Hydrolysis. There are 19 different chemical bonds for the five remaining anion candidates, which lead to 19 potential hydrolytic reactions. The reaction enthalpy and barrier heights are shown in Figure 5. Of these, six reactions—in which all of them involve a N−P, Si−F, or N−Si bond—are strongly endothermic and, hence, unlikely to occur. The barrier heights were calculated for both the S_N1 and the S_N2 pathways for the remaining 13 hydrolytic reactions. Particularly, for the S_N2 mechanism, six reactions were found to follow a single transition state pathway and the other seven reactions were found to follow a double transition state pathway. Except for the BDMTSA C−F bond, all S_N2 barrier heights were lower than the S_N1 barrier height. It can be concluded that most of the hydrolytic reactions (if feasible) favor the S_N2 mechanism except in the case of BDMTSA C−F, which favors the S_N1 mechanism.

The first class of anions, including BFTMPA, BDMTSA, DTPA, and MDPA, are associated with high hydrolytic barriers for both the S_N1 and S_N2 pathways, where the minimum barrier height is as high as 0.96 eV. On the basis of these barrier heights, we surmise that the reaction rate constants are negligible. Furthermore, the water concentration in the nonaqueous electrolytes is usually quite low (<100 ppm), and hence, hydrolysis is unlikely to contribute to significant electrolyte degradation for these four anions. The second anion class contains only one anion, BDDFSA, which exhibits the Si−C bond as the most vulnerable to hydrolysis. Its barrier height is 0.77 eV, which is 0.10 eV lower than our criteria. Therefore, BDDFSA is excluded due to potential hydrolysis vulnerability. In summary, through our systematic and comprehensive computational screening of electrochemical and chemical stability as well as hydrolysis, we find BFTMPA, BDMTSA, DTPA ,and MDPA to be promising novel anion candidates.

4.4. Miscellaneous. Although the theoretical screening process indicates that BFTMPA, BDMTSA, DTPA, and MDPA are promising electrolyte salt candidates, we caution that there may be other considerations that are pertinent to observe before attempting synthesis. For example, BFTMPA shares a structural similarity with sarin,[42] which is a notorious toxic agent. As a result, we would rule out BFTMPA for experimental investigation but nevertheless kept the results as part of the paper as its structure and chemical stability may inspire other ideas. As for TFSTSA and BTFMSA, which have been shown to have poor electrochemical windows, we observe that they are both essentially silanones. Silanone is highly unstable even at low temperatures, and it is well known that such compounds can undergo rapid head-to-tail-polymerization to give polysiloxanes $(R_2SiO)_n$ (silicone, a common sealant).[43] Therefore, even excluding our assessment of their electrochemical instability, these anions are unlikely to be good candidates for electrolyte applications.

4.5. Liquid Structure and Transport Properties. The remaining anion candidates BDMTSA, DTPA, and MDPA were further studied using classical MD simulations in various solvent solutions (AN, THF, DMSO, G1, G2, G4). Before calculating the properties of the electrolyte solutions, the densities of the pure solvents were studied as a validation of the force fields. For the six solvents, the calculated densities at 298 K are shown in Table 2. As shown in the table, all the densities agree well with experimental results.

On the basis of the NVT ensemble simulations, the liquid-phase structure in each solution was analyzed in terms of its radial distribution functions (RDFs). Using these RDFs, the coordination numbers of anion and solvent molecules in the first solvation shell of the Mg^{2+} ion were calculated for each solution. The first solvation shell was defined as the minimum between the first and second maximum in the corresponding RDF. The calculated coordination numbers for Mg^{2+}∼N (in anion) and Mg^{2+}∼N/O (in solvent) are shown in Figure 6. The results for the TFSI anion solutions are also provided for comparison. Due to the use of a different force field, the TFSI results are not identical but still consistent and in qualitative

DOI: 10.1021/acs.jpcc.7b04516
J. Phys. Chem. C 2017, 121, 16126−16136

Table 2. Calculated Density of Pure Solvent at 298 K Compared with Experimental Results[a]

solvent	calculated density (g/cm^3)	experimental density (g/cm^3)	error%
AN	0.788	0.777	1.381
THF	0.886	0.882	0.424
DMSO	1.127	1.096	2.834
G1	0.871	0.861	1.124
G2	0.938	0.939	−0.081
G4	0.986	1.007	−2.096

[a]The uncertainties in the calculated densities are less than 0.001 g/cm^3.

agreement with the results reported in our previous publication.[24] As shown in Figure 6, in almost all solutions of DTPA and MDPA anions (see below), the coordination numbers between Mg^{2+} and anions are between 1.0 and 2.0, similar to the case of the TFSI anion solutions, whereas Mg^{2+} and BDMTSA anions tend to have coordination numbers smaller than 1.0. No coordination numbers significantly larger than 2.0 were observed in these solutions. In most solutions, solvent molecules coordinate more with the Mg^{2+} ions than anions do. Total coordination numbers (anion + solvent) of up to six were observed in the solutions.

It is worth mentioning that the difference in the calculated coordination numbers can be caused by the different cutoff distances for the first solvation shell in each solution due to the different coordination structure and the fact that the chosen atoms do not necessarily represent the preferred coordination sites in all solutions. Because of this, we also computed the overall coordination number for Mg^{2+} for all of the atom types in the solution. The result is shown in Figure 7. In all solutions, the cutoff distances for the first solvation shell are similar

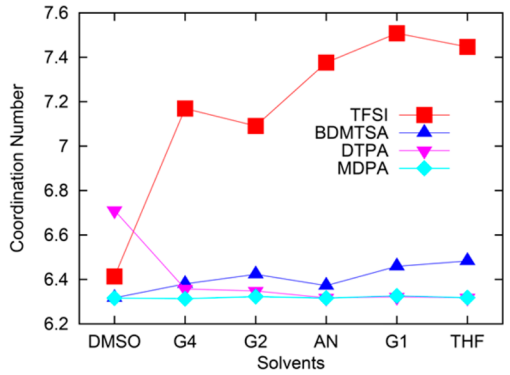

Figure 7. Calculated overall coordination number of Mg^{2+} ions in the four electrolyte solutions at 298 K.

(between 2.5 and 2.9 Å). For TFSI, the overall coordination number can be up to 7.5 depending on the solvent. For most of the new anion solutions, the total coordination numbers of Mg^{2+} are ≈6 (e.g., octahedral). Except for DTPA in DMSO, the Mg^{2+} are less coordinated by the new anions than TFSI. For most solvents, the coordination numbers in DTPA and MDPA anion solutions are smaller than those in BDMTSA. The same trend was observed when the same cutoff distances of 2.8 Å were applied in all solutions (results not shown). One might expect that lower coordination numbers will lead to faster dynamics of the Mg^{2+} ions. However, as shown below, the correlation between the liquid structure and its dynamics is not simple, which points to the need of more sophisticated models.

The dynamic properties of the electrolyte solutions were studied. The self-diffusion coefficients of the cation and anion in each solution (see Figure 8) were calculated using the Einstein relation. The dynamics in the pure G4 solution were

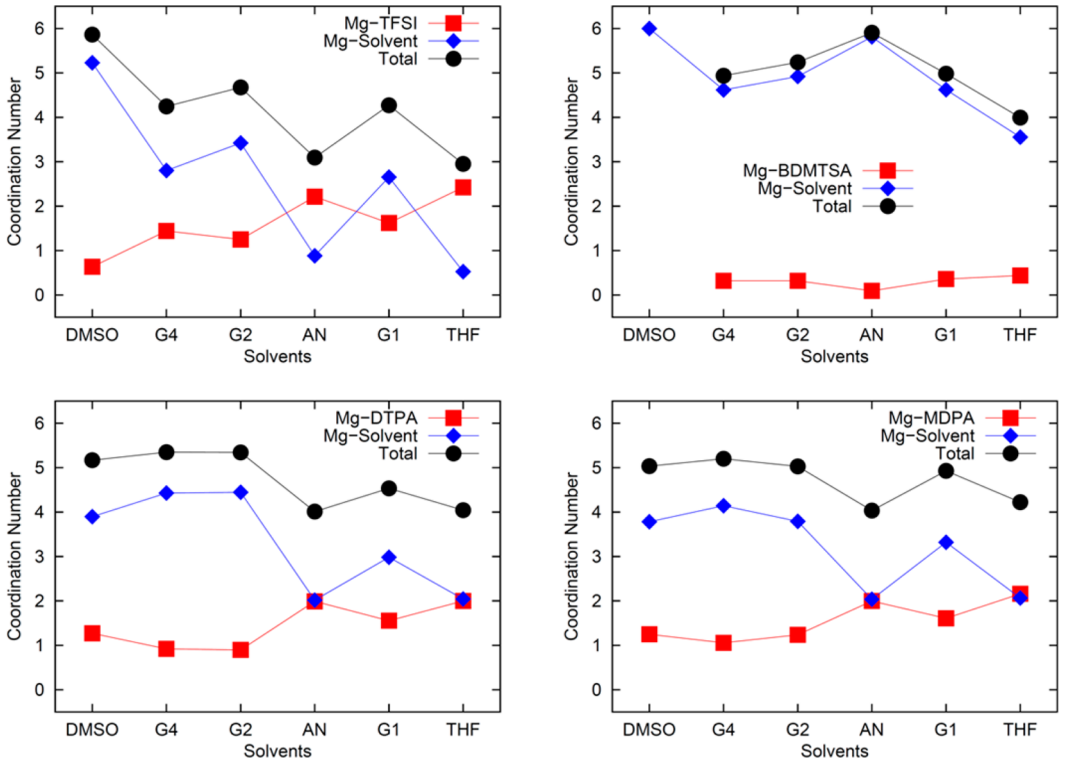

Figure 6. Calculated coordination number of the four electrolytes in six solvents at 298 K.

DOI: 10.1021/acs.jpcc.7b04516
J. Phys. Chem. C 2017, 121, 16126−16136

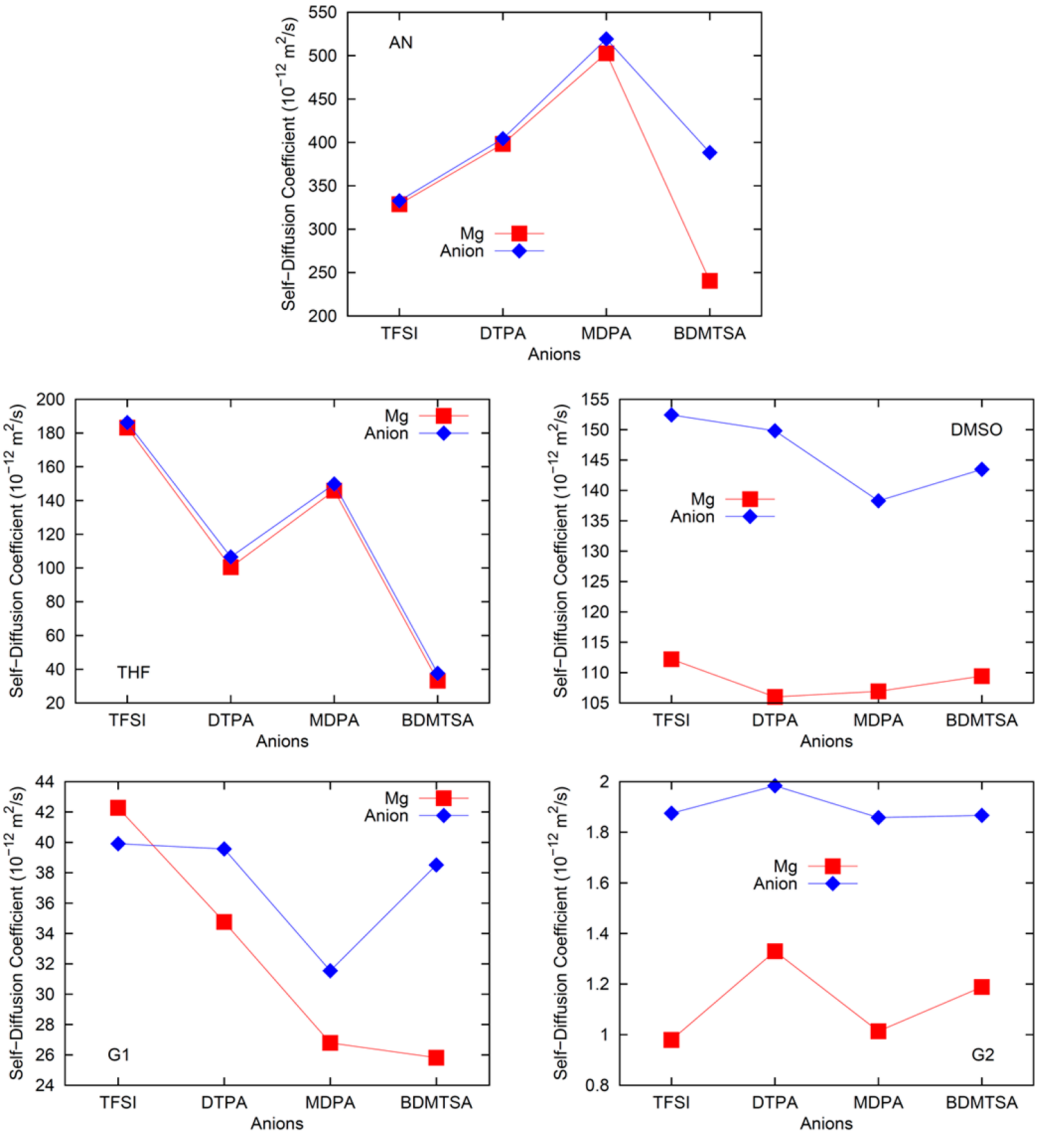

Figure 8. Calculated self-diffusion coefficients using the Einstein relation at 298 K.

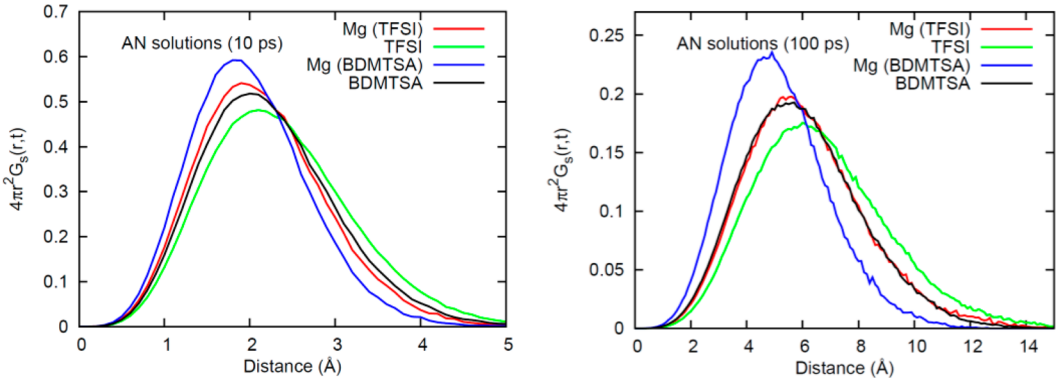

Figure 9. Calculated self-part of the van Hove function of cations and anions of Mg^{2+}/TFSI/AN and Mg^{2+}/BDMTSA/AN solutions at 10 ps (left) and 100 ps (right).

too slow to reach the normal diffusion region over the time scale of the simulations and are thus not shown. In almost all of the solutions, the anions were found to have larger diffusivities than Mg^{2+}, despite the fact that the anions are larger than Mg^{2+}. This is well known and correlates with results from the Li-ion electrolytes.[44−49] In THF solutions, cations and anions have almost the same diffusivity, consistent with the relatively large cation−anion coordination number in these solutions. For a given solvent, the dynamics of cations and anions are least correlated in the BDMTSA solutions. While it is possible to

DOI: 10.1021/acs.jpcc.7b04516
J. Phys. Chem. C 2017, 121, 16126−16136

compare the dynamics of a given solvent with different anions, which is one of the goals of this work, it is not possible to make reliable comparisons of the dynamics of a given anion in different solvents, due to the variation in solvent force fields.

While self-diffusion coefficients describe the averaged dynamics of a given ion type, it is also of interest to study the distribution of their dynamics. This can be quantified by computing the self-part of the van Hove function,[50,51] given by

$$G_S(r, t) = \frac{1}{N}\langle \sum_{1}^{N} \delta(r_i(t) - r_i(0) - r)\rangle$$

which measures the probability that an ion has moved a distance r within the time t. Figure 9 shows the calculated van Hove function of TFSI and BDMTSA salts in the AN solutions at 10 ps (top) and 100 ps (bottom), respectively. As shown in the plots, the van Hove function has a single peak in all cases but whose position moves to longer distances as time increases, indicating diffusive motion. At a given time, the peak positions of the anion are located at longer distances than that of the cation in both solutions, indicating that the anions have faster dynamics than the cations, consistent with the calculated self-diffusion coefficients shown in Figure 8. In Figure 9, the tails at long distance in the calculated van Hove function represent faster dynamics, which is only a small fraction of anions in each solution. The dynamics of the majority of the cations and anions are similar, and their distributions overlap, indicating similar dynamic properties. The van Hove function results in other solutions or at other times show similar behavior and are not shown here.

The ionic conductivity of each solution was estimated using the Nernst−Einstein relation. The results are shown in Figure 10. Similar to the self-diffusion coefficients, the relative ionic conductivities of the four electrolyte solutions depend on the solvents.

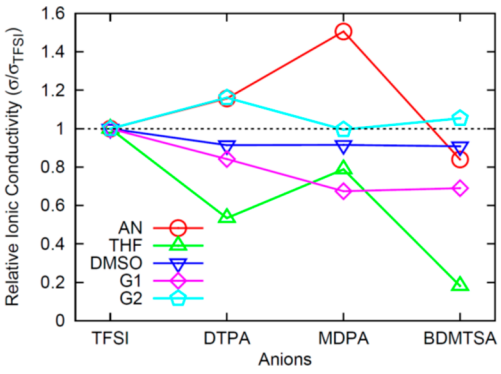

Figure 10. Estimated ionic conductivity using the Nernst−Einstein relation at 298 K. The results are normalized to that in TFSI solutions.

In summary, in the new electrolytes, the Mg^{2+} ions were found to form similar or less contact-ion pairs than in the TFSI solution. As expected, the transport properties are solvent dependent in all cases, but generally, the transport properties of the new electrolytes are comparable to those of the parent TFSI solutions. However, the conductivities of BDMTSA solutions are found to be worse than TFSI solutions in most solvents. Therefore, BDMTSA is removed from the list and DTPA and MDPA are finally recommended for further consideration and potential experimental exploration. DTPA and MDPA show significantly improved chemical stability under charge-transfer conditions and, hence, may inhibit the interfacial film formation which is exhibited by $Mg(TFSI)_2$, while all other considered properties are as good as or improved as compared to TFSI.

CONCLUSIONS

We demonstrate a comprehensive computational design of novel electrolyte salts, using a tiered-screening approach and combining first-principles and classical molecular dynamics methods. Specifically, we use a previously identified decomposition mechanism for $TFSI^-$, which is based on the chemical reactivity when ion-paired with the transient Mg^+, and propose target substitutions that show increased stability as compared to the original anion. The substitution strategy resulted in 15 proposed new anions, which were considered as candidates for multivalent electrolyte systems. To screen for the most promising candidates, we calculated the electrochemical stability window, chemical stability, hydrolysis tolerance, and the transport properties in a Mg-electrolyte setting. Two anions, DTPA and MDPA, are found to show greatly improved chemical stability over TFSI, while none of the other considered properties were found to deteriorate. This work shows, to our knowledge, the first rational design of electrolytes through computational insights. The results presented are recommended for experimental exploration and inspiration toward improved performance of multivalent-ion electrolytes.

ASSOCIATED CONTENT

Supporting Information

The Supporting Information is available free of charge on the ACS Publications website at DOI: 10.1021/acs.jpcc.7b04516.

Bond dissociation energy for all of the bonds in BDDFSA and Benchmark result with explicit solvent model (PDF)

AUTHOR INFORMATION

Corresponding Author

*E-mail: kapersson@lbl.gov.

ORCID

Xiaohui Qu: 0000-0001-5651-8405
Yong Zhang: 0000-0003-3988-5961
Nav Nidhi Rajput: 0000-0003-4740-8217
Edward Maginn: 0000-0002-6309-1347

Author Contributions

#X.Q. and Y.Z. contributed equally to this work.

Notes

The authors declare no competing financial interest.

ACKNOWLEDGMENTS

Support for this work came from the U.S. Department of Energy, Basic Energy Science, Joint Center for Energy Storage Research under Contract No. DE-AC02-06CH11357. The calculations were performed using the computational resources of the National Energy Research Scientific Computing Center, which is supported by the Office of Science of the U.S. Department of Energy under Contract No. DE-AC02-05CH11231. The Materials Project (BES DOE Grant No. EDCBEE) is acknowledged for infrastructure and algorithmic support. We gratefully thank Dr. Anthony K. Burrell at Argonne National Laboratory (United States) for valuable discussions.

DOI: 10.1021/acs.jpcc.7b04516
J. Phys. Chem. C 2017, 121, 16126−16136

REFERENCES

(1) Christensen, J.; Albertus, P.; Sanchez-Carrera, R. S.; Lohmann, T.; Kozinsky, B.; Liedtke, R.; Ahmed, J.; Kojic, A. A Critical Review of Li/Air Batteries. *J. Electrochem. Soc.* **2012**, *159*, R1−R30.

(2) Shao, Y.; Ding, F.; Xiao, J.; Zhang, J.; Xu, W.; Park, S.; Zhang, J. G.; Wang, Y.; Liu, J. Making Li-Air Batteries Rechargeable: Material Challenges. *Adv. Funct. Mater.* **2013**, *23*, 987−1004.

(3) Abraham, K. M. Prospects and Limits of Energy Storage in Batteries. *J. Phys. Chem. Lett.* **2015**, *6*, 830−844.

(4) Doe, R. E.; Han, R.; Hwang, J.; Gmitter, A. J.; Shterenberg, I.; Yoo, H. D.; Pour, N.; Aurbach, D. Novel, Electrolyte Solutions Comprising Fully Inorganic Salts with High Anodic Stability for Rechargeable Magnesium Batteries. *Chem. Commun.* **2014**, *50*, 243−245.

(5) Muldoon, J.; Bucur, C. B.; Oliver, A. G.; Sugimoto, T.; Matsui, M.; Kim, H. S.; Allred, G. D.; Zajicek, J.; Kotani, Y. Electrolyte Roadblocks to a Magnesium Rechargeable Battery. *Energy Environ. Sci.* **2012**, *5*, 5941−5950.

(6) Kim, H. S.; Arthur, T. S.; Allred, G. D.; Zajicek, J.; Newman, J. G.; Rodnyansky, A. E.; Oliver, A. G.; Boggess, W. C.; Muldoon, J. Structure and Compatibility of a Magnesium Electrolyte with a Sulphur Cathode. *Nat. Commun.* **2011**, *2*, 427.

(7) Keyzer, E. N.; Glass, H. F. J.; Liu, Z.; Bayley, P. M.; Dutton, S. E.; Grey, C. P.; Wright, D. S. $Mg(PF_6)_2$ Based Electrolyte Systems: Understanding Electrolyte−Electrode Interactions for the Development of Mg-Ion Batteries. *J. Am. Chem. Soc.* **2016**, *138*, 8682−8685.

(8) Lu, Z.; Schechter, A.; Moshkovich, M.; Aurbach, D. On the Electrochemical Behavior of Magnesium Electrodes in Polar Aprotic Electrolyte Solutions. *J. Electroanal. Chem.* **1999**, *466*, 203−217.

(9) Arthur, T. S.; Singh, N.; Matsui, M. Electrodeposited Bi, Sb and $Bi_{1-x}Sb_x$ Alloys as Anodes for Mg-Ion Batteries. *Electrochem. Commun.* **2012**, *16*, 103−105.

(10) Tran, T. T.; Lamanna, W. M.; Obrovac, M. N. Evaluation of $Mg[N(SO_2CF_3)_2]_2$/Acetonitrile Electrolyte for Use in Mg-Ion Cells. *J. Electrochem. Soc.* **2012**, *159*, A2005−A2009.

(11) Ha, S.; Lee, Y. W.; Woo, S. W.; Koo, B.; Kim, J.; Cho, J.; Lee, K. T.; Choi, N. Magnesium(II) Bis(trifluoromethane Sulfonyl) Imide Based Electrolytes with Wide Electrochemical Windows for Rechargeable Magnesium Batteries. *ACS Appl. Mater. Interfaces* **2014**, *6*, 4063−4073.

(12) Schwarz, R.; Pejic, M.; Fischer, P.; Marinaro, M.; Jörissen, L.; Wachtler, M. Magnesocene-Based Electrolytes: A New Class of Electrolytes for Magnesium Batteries. *Angew. Chem., Int. Ed.* **2016**, *55*, 14958−14962.

(13) Tutusaus, O.; Mohtadi, R.; Singh, N.; Arthur, T. S.; Mizuno, F. Study of Electrochemical Phenomena Observed at the Mg Metal/Electrolyte Interface. *ACS Energy Lett.* **2017**, *2*, 224−229.

(14) Saha, P.; Datta, M. K.; Velikokhatnyi, O. I.; Manivannan, A.; Alman, D.; Kumta, P. N. Rechargeable Magnesium Battery: Current Status and Key Challenges for the Future. *Prog. Mater. Sci.* **2014**, *66*, 1−86.

(15) Yoo, H. D.; Shterenberg, I.; Gofer, Y.; Gershinsky, G.; Pour, N.; Aurbach, D. Mg Rechargeable Batteries: An On-going Challenge. *Energy Environ. Sci.* **2013**, *6*, 2265−2279.

(16) Aurbach, D.; Suresh, G. S.; Levi, E.; Mitelman, A.; Mizrahi, O.; Chusid, O.; Brunelli, M. Progress in Rechargeable Magnesium Battery Technology. *Adv. Mater.* **2007**, *19*, 4260−4267.

(17) Aurbach, D.; Lu, Z.; Schechter, A.; Gofer, Y.; Gizbar, H.; Turgeman, R.; Cohen, Y.; Moshkovich, M.; Levi, E. Prototype Systems for Rechargeable Magnesium Batteries. *Nature* **2000**, *407*, 724−727.

(18) Shterenberg, I.; Salama, M.; Gofer, Y.; Levi, E.; Aurbach, D. The Challenge of Developing Rechargeable Magnesium Batteries. *MRS Bull.* **2014**, *39*, 453−460.

(19) Salama, M.; Shterenberg, I.; Gizbar, H.; Eliaz, N. N.; Kosa, M.; Keinan-Adamsky, K.; Afri, M.; Shimon, L. J. W.; Gottlieb, H. E.; Major, D. T.; et al. Unique Behavior of Dimethoxyethane (DME)/$Mg(N(SO_2CF_3)_2)_2$ Solutions. *J. Phys. Chem. C* **2016**, *120*, 19586−19594.

(20) Song, J.; Sahadeo, E.; Noked, M.; Lee, S. B. Mapping the Challenges of Magnesium Battery. *J. Phys. Chem. Lett.* **2016**, *7*, 1736−1749.

(21) Kim, D. Y.; Lim, Y.; Roy, B.; Ryu, Y. G.; Lee, S. S. Operating Mechanisms of Electrolytes in Magnesium Ion Batteries: Chemical Equilibrium, Magnesium Deposition, and Electrolyte Oxidation. *Phys. Chem. Chem. Phys.* **2014**, *16*, 25789−25798.

(22) Aurbach, D.; Lu, Z.; Schechter, A.; Gofer, Y.; Gizbar, H.; Turgeman, R.; Cohen, Y.; Moshkovich, M.; Levi, E. Prototype Systems for Rechargeable Magnesium Batteries. *Nature* **2000**, *407*, 724−727.

(23) Tutusaus, O.; Mohtadi, R.; Arthur, T. S.; Mizuno, F.; Nelson, E. G.; Sevryugina, Y. V. An Efficient Halogen-Free Electrolyte for Use in Rechargeable Magnesium Batteries. *Angew. Chem., Int. Ed.* **2015**, *54*, 7900−7904.

(24) Rajput, N. N.; Qu, X.; Sa, N.; Burrell, A. K.; Persson, K. A. The Coupling between Stability and Ion Pair Formation in Magnesium Electrolytes from First-Principles Quantum Mechanics and Classical Molecular Dynamics. *J. Am. Chem. Soc.* **2015**, *137*, 3411−3420.

(25) Shao, Y.; Liu, T.; Li, G.; Gu, M.; Nie, Z.; Engelhard, M.; Xiao, J.; Lv, D.; Wang, C.; Zhang, J. G. Coordination Chemistry in Magnesium Battery Electrolytes: How Ligands Affect Their Performance. *Sci. Rep.* [Online], **2013**, *3*. DOI: 10.1038/srep03130.

(26) *MarvinSketch*, version 15.1.12.0; ChemAxon, Ltd.: Budapest, Hungary, 2015. (Advanced chemical editor for drawing chemical structures, queries, and reactions.)

(27) Watkins, T.; Buttry, D. A. Determination of Mg^{2+} Speciation in a TFSI Based Ionic Liquid With and Without Chelating Ethers Using Raman Spectroscopy. *J. Phys. Chem. B* **2015**, *119*, 7003−7014.

(28) Baskin, A.; Prendergast, D. Exploration of the Detailed Conditions for Reductive Stability of $Mg(TFSI)_2$ in Diglyme: Implications for Multivalent Electrolytes. *J. Phys. Chem. C* **2016**, *120*, 3583−3594.

(29) Tomasi, J.; Mennucci, B.; Cancès, E. The IEF Version of the PCM Solvation Method: An Overview of a New Method Addressed to Study Molecular Solutes at the QM Ab Initio Level. *J. Mol. Struct.: THEOCHEM* **1999**, *464*, 211−226.

(30) Qu, X.; Jain, A.; Rajput, N. N.; Cheng, L.; Zhang, Y.; Ong, S. P.; Brafman, M.; Maginn, E.; Curtiss, L. A.; Persson, K. A. The Electrolyte Genome Project: A Big Data Approach in Battery Materials Discovery. *Comput. Mater. Sci.* **2015**, *103*, 56−67.

(31) Cheng, L.; Assary, R. S.; Qu, X.; Jain, A.; Ong, S. P.; Rajput, N. N.; Persson, K.; Curtiss, L. A. Accelerating Electrolyte Discovery for Energy Storage with High Throughput Screening. *J. Phys. Chem. Lett.* **2015**, *6*, 283−291.

(32) Plimpton, S. Fast Parallel Algorithms for Short-Range Molecular Dynamics. *J. Comput. Phys.* **1995**, *117*, 1−19.

(33) Maginn, E. J. Molecular Simulation of Ionic Liquids: Current Status and Future Opportunities. *J. Phys.: Condens. Matter* **2009**, *21*, 373101.

(34) Zhang, Y.; Maginn, E. J. Direct Correlation between Ionic Liquid Transport Properties and Ion Pair Lifetimes: A Molecular Dynamics Study. *J. Phys. Chem. Lett.* **2015**, *6*, 700−705.

(35) Wang, J. M.; Wolf, R. M.; Caldwell, J. W.; Kollman, P. A.; Case, D. A. Development and Testing of a General Amber Force Field. *J. Comput. Chem.* **2004**, *25*, 1157−1174.

(36) Frisch, M. J.; Trucks, G. W.; Schlegel, H. B.; Scuseria, G. E.; Robb, M. A.; Cheeseman, J. R.; Scalmani, G.; Barone, V.; Mennucci, B.; Petersson, G. A.; Nakatsuji, H.; Caricato, M.; Li, X.; Hratchian, H. P.; Izmaylov, A. F.; Bloino, J.; Zheng, G.; Sonnenberg, J. L.; Hada, M.; Ehara, M.; Toyota, K.; Fukuda, R.; Hasegawa, J.; Ishida, M.; Nakajima, T.; Honda, Y.; Kitao, O.; Nakai, H.; Vreven, T.; Montgomery, J. A., Jr.; Peralta, J. E.; Ogliaro, F.; Bearpark, M.; Heyd, J. J.; Brothers, E.; Kudin, K. N.; Staroverov, V. N.; Kobayashi, R.; Normand, J.; Raghavachari, K.; Rendell, A.; Burant, J. C.; Iyengar, S. S.; Tomasi, J.; Cossi, M.; Rega, N.; Millam, J. M.; Klene, M.; Knox, J. E.; Cross, J. B.; Bakken, V.; Adamo, C.; Jaramillo, J.; Gomperts, R.; Stratmann, R. E.; Yazyev, O.; Austin, A. J.; Cammi, R.; Pomelli, C.; Ochterski, J. W.; Martin, R. L.; Morokuma, K.; Zakrzewski, V. G.; Voth, G. A.; Salvador, P.; Dannenberg, J. J.; Dapprich, S.; Daniels, A. D.; Farkas, O.;

DOI: 10.1021/acs.jpcc.7b04516
J. Phys. Chem. C 2017, 121, 16126−16136

Foresman, J. B.; Ortiz, J. V.; Cioslowski, J.; Fox, D. J. *Gaussian 09*, revision D.01; Gaussian, Inc.: Wallingford, CT, 2009.
(37) Bayly, C. I.; Cieplak, P.; Cornell, W. D.; Kollman, P. A. A Well-Behaved Electrostatic Potential Based Method Using Charge Restraints for Deriving. *J. Phys. Chem.* **1993**, *97*, 10269−10280.
(38) Hockney, R.; Eastwood, J. *Computer Simulation Using Particles*; Taylor & Francis Group: New York, 1988.
(39) Tsuzuki, S.; Shinoda, W.; Matsugami, M.; Umebayashi, Y.; Ueno, K.; Mandai, T.; Seki, S.; Dokko, K.; Watanabe, M. Structures of $[Li(glyme)]^+$ Complexes and Their Interactions with Anions in Equimolar Mixtures of Glymes and Li[TFSA]: Analysis by Molecular Dynamics Simulations. *Phys. Chem. Chem. Phys.* **2015**, *17*, 126−129.
(40) Jorgensen, W. L.; Maxwell, D. S.; Tirado-Rives, J. Development and Testing of the OPLS All-Atom Force Field on Conformational Energetics and Properties of Organic Liquids. *J. Am. Chem. Soc.* **1996**, *118*, 11225−11236.
(41) Del Monte, F.; Mackenzie, J. D.; Levy, D. Rhodamine Fluorescent Dimers Adsorbed on the Porous Surface of Silica Gels. *Langmuir* **2000**, *16*, 7377−7382.
(42) Abu-Qare, A. W.; Abou-Donia, M. B. Sarin: Health Effects, Metabolism, and Methods of Analysis. *Food Chem. Toxicol.* **2002**, *40*, 1327−1333.
(43) Tokitoh, N.; Okazaki, R. Recent Advances in the Chemistry of Silicon-Heteroatom Multiple Bonds. In *The Chemistry of Organic Silicon Compounds*; Rappoport, Z., Apeloig, Y., Eds.; PATAI'S Chemistry of Functional Groups; John Wiley & Sons: Chichester, U.K., 1998; Vol. 2, pp 1063−1103.
(44) Borodin, O.; Smith, G. D.; Henderson, W. Li^+ Cation Environment, Transport, and Mechanical Properties of the LiTFSI Doped N-Methyl-N-Alkylpyrrolidinium$^+$TFSI$^-$ Ionic Liquids. *J. Phys. Chem. B* **2006**, *110*, 16879−16886.
(45) Monteiro, M. J.; Bazito, F. F. C.; Siqueira, L. J. A; Ribeiro, M. C. C.; Torresi, R. M. Transport Coefficients, Raman Spectroscopy, and Computer Simulation of Lithium Salt Solutions in an Ionic Liquid. *J. Phys. Chem. B* **2008**, *112*, 2102−2109.
(46) Bayley, P. M.; Best, A. S.; MacFarlane, D. R.; Forsyth, M. The Effect of Coordinating and Non-Coordinating Additives on the Transport Properties in Ionic Liquid Electrolytes for Lithium Batteries. *Phys. Chem. Chem. Phys.* **2011**, *13*, 4632−4640.
(47) Castiglione, F.; Ragg, E.; Mele, A.; Appetecchi, G. B.; Montanino, M.; Passerini, S. Molecular Environment and Enhanced Diffusivity of Li^+ Ions in Lithium-Salt-Doped Ionic Liquid Electrolytes. *J. Phys. Chem. Lett.* **2011**, *2*, 153−157.
(48) Liao, C.; Shao, N.; Han, K. S.; Sun, X. G.; Jiang, D.-E.; Hagaman, E. W.; Dai, S. Physicochemical Properties of Imidazolium-Derived Ionic Liquids with Different C-2 Substitutions. *Phys. Chem. Chem. Phys.* **2011**, *13*, 21503.
(49) Liu, H.; Maginn, E. Effect of Ion Structure on Conductivity in Lithium-Doped Ionic Liquid Electrolytes: A Molecular Dynamics Study. *J. Chem. Phys.* **2013**, *139*, 114508.
(50) Del Pópolo, M. G.; Voth, G. A. On the Structure and Dynamics of Ionic Liquids. *J. Phys. Chem. B* **2004**, *108*, 1744−1752.
(51) Jiang, W.; Yan, T.; Wang, Y.; Voth, G. A. Molecular Dynamics Simulation of the Energetic Room-Temperature Ionic Liquid, 1-Hydroxyethyl-4-Amino-1,2,4-Triazolium Nitrate (HEATN). *J. Phys. Chem. B* **2008**, *112*, 3121−3131.

DOI: 10.1021/acs.jpcc.7b04516
J. Phys. Chem. C 2017, 121, 16126−16136